New Hybrid Ray-Tracing/FDTD for EMF Exposure in 6G Networks using Semantically Classified Google Earth Photogrammetry with Measurement Validation

Robin Wydaeghe, Arno Moerman, Olivier Caytan, Sergei Shikhantsov, Emmeric Tanghe,
Günter Vermeeren, Hendrik Rogier, Sam Lemey, Piet Demeester, Wout Joseph
Department of Information Technology, Ghent University/IMEC, WAVES & IDLab, Ghent, Belgium, Robin.Wydaeghe@UGent.be

***Abstract*—State-of-the-art (SOTA) technologies are combined to make channel and exposure assessment in realistic environments anywhere on Earth a reality. The new API for 3D photorealistic tiles from the Google Earth dataset provides high Level of Detail (LoD) and high coverage photogrammetry. These meshes are semantically classified with a SOTA deep-learning model to distinguish classes such as buildings, terrain and vegetation. The environment is ray-traced at 26 GHz millimeter waves (mmWaves) with a 6G distributed massive MIMO (DMaMIMO) antenna system as Tx and omnidirectional User Equipment (UE) as Rx. The latter provides input for a hybridization procedure that models the Electromagnetic Fields (EMFs) around the UE. The new surface absorbed power density S_{ab} exposure metric is can be computed along the path using Finite-Difference Time-Domain (FDTD) simulations. A scan measurement from an in-house beamforming 16-element DMaMIMO antenna system in an anechoic room is performed with the new FR2 probe from NARDA. The EMFs of the created hotspot are compared with results from the hybridization component in the simulation pipeline, with a 1D Normalized Mean Absolute Error (NMAE) of 17%. The measurement validates the use of the simulations in realistic environments. A case-study near Central Park in New York City, USA, is examined. Ray-tracing the environment is shown to be feasible with the processed mesh and S_{ab} computations indicate compliance with the ICNIRP guidelines.**

***Index Terms*—realistic exposure, photogrammetry, semantic classification, ray-tracing, measurement, simulation, surface absorbed power density, 5G, mmWave, 6G, distributed massive MIMO**

I. Introduction

A. Scope

The fifth generation of telecommunication (5G) aims to increase spectral efficiency and data rates. Among the enabling technologies are (1) massive MIMO (MaMIMO), antennas composed of a large number of elements, and (2) the utilization of higher frequencies, such as millimeter waves (mmWaves). For the former, beamforming becomes possible by constructively interfering each element's wavefront through phase modulation. Beamforming actively concentrates the emitted radiation optimally towards the User Equipment (UE), in contrast with fourth-generation (4G) base stations which do not alter the channel. For the latter, higher bandwidths become available in unlicensed frequency bands, such as FR2, which operates around 26 GHz. However, these higher frequencies incur greater path loss. One potential solution are sixth-generation (6G) Distributed MaMIMO (DMaMIMO) base stations. Elements are distributed, e.g., on a building facade, reducing the path length to the UE.

To achieve *active* beamforming at high frequencies, the channel between receiver (Rx) and transmitter (Tx) must be precoded. For line-of-sight (LOS) transmission scenarios, this causes (a) the direction of maximal gain to be aligned towards the Rx and (b) the individual element's phases of the Tx to constructively interfere at the location of the UE. In the case of *passive* beamforming, also known as codebook-based beamforming, only the former will be true as the exact channel is not known. When several incoming electromangetic-field (EMF) beams impinge on the UE, either from non-line-of-sight (NLOS) scattering or a DMaMIMO antenna, a hotspot of increased EMF can arise at the location of the UE. The nature of these hotspots is not well-known, in particular for the active beamforming scenario. Due to constructive interference, a wavelength-sized region can have increased EMF [1]. It is of particular importance to study the effects of these hotspots on EMF exposure on humans, asserting that they comply with the international limits, e.g., set by the International Commission on Non-Ionizing Radiation Protection (ICNIRP). ICNIRP updated its guidelines in 2020. A new surface absorbed power density metric S_{ab} [2] is introduced for frequencies above 6 GHz. Worst-case exposure assessment is well-studied. however, *realistic* exposure assessment for 5G and 6G cellular networks is lacking. Simulating actual exposure levels is important not only from a public health and awareness perspective, but also to plan the locations and powers of base stations in future networks. To model the exposure from hotspots in modern technologies, the propagation step needs to be interfaced with the exposure step in one integrated method [3].

B. Structure and novelties

A flowchart in Fig. 1 illustrates the structure of this paper.

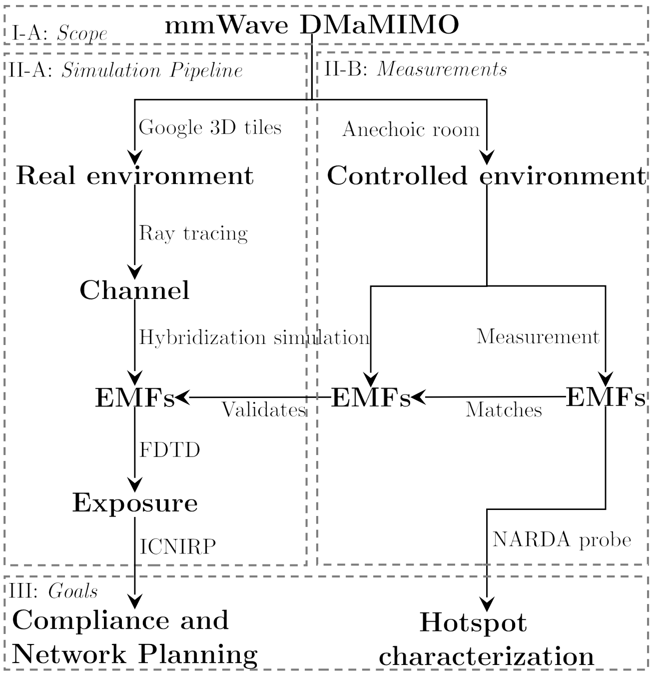

Fig. 1. A flowchart of this paper. The dotted boxes correspond to different sections. Hybridization simulations are performed for the EMFs in both section II-A and II-B

The *simulations* in this paper were facilitated by three recent developments.

1) In 2023, Google released their API for photorealistic 3D tiles to the public. The database is well-known as the provider of Google Earth and Google Maps 3D imagery. The combination of its high Level of Detail (LoD) with a world-wide coverage is industry-leading. For the first time, these tiles are used in a scientific publication. For this, we present a method to process the raw data to a suitable mesh for ray-tracing.
2) A 2021 SOTA deep-learning technique from 2021 is sufficiently reliable to semantically label photogrammetry meshes. For the first time, a high-accuracy semantic classifier is applied to high-LoD high-coverage photogrammetry.
3) In 2022, hybrid ray-tracing/FDTD was extended to 26 GHz mmWave frequencies and 6G networks in [3]. Now, the accuracy of the hybridizer is improved by using a Huygens box. The new S_{ab} EMF exposure metric is evaluated in highly realistic outdoor environments at 26 GHz.

This paper implements these developments in one pipeline, as shown in Fig. 1. Together, channel modeling and exposure assessment can now be studied at any location covered by Google Earth. The method is specifically applied to the 6G DMaMIMO paradigm at 26 GHz mmWaves. A case-study in New York City, USA, is shown as a proof-of-concept.

The *measurements* in this paper were facilitated by new, optimized and easy-to-use equipment. In the final propagation between the Last-Bounce-Scatterer (LBS) and the UE, the EMFs are evaluated on a Huygens box around the UE. For the first time, this area was scanned in high resolution in an anechoic room at 26 GHz with a DMaMIMO Tx system. The EMFs from the simulations matches deterministically with the EMFs from the measurement. This match validates the new hybridization component of the simulation pipeline. The simulation in this controlled environment adds credibility to simulations in realistic real environments. Moreover, the measurement provides a multi-dimensional field map of a 26 GHz hotspot, extending the work from Shikhantsov *et al.* at 3.5 GHz [4].

II. Methods

A. Simulation Pipeline

1) Environments: For high accuracy ray-tracing simulations, a high accuracy environment is essential. In particular for mmWave frequencies, it is not sufficient to model building facades as flat surfaces [5] or roads street canyons without cars or lampposts [6]. Foliage is rarely modeled with individual trees. The wavelength at 26 GHz is 1.15 cm. Therefore, centimeter-sized features significantly affect the diversity of the channel. A greater number of NLOS paths can be utilized to beamform the signal towards the UE. At the 2023 Google I/O conference, Google released their API for photorealistic 3D tiles to the public in an experimental phase [7]. A free Google API key provides access to all photogrammetry data in the 3D OGC tiles format. This method is applicable to any location 3D-mapped by Google Earth, which includes nearly all major western cities as well as vast suburban areas. Alternatives either do not provide the same level of coverage (e.g. Bing Maps) or LoD (e.g. Open Street Maps). We present a three-step method that processes the raw data to a suitable mesh for ray-tracing.

In the first step, we stream data at the highest LoD with a Blender renderer [8]. The result is a textured mesh. Common artifacts of photogrammetry data are present: non-manifold vertices and edges, duplicate vertices and faces, non-contiguous edges, and more. Moreover, some low-detail features contain an unnecessary amount of vertices, in particular at the seams of tiles. Therefore, the mesh quality is improved and its size is reduced.

1) The region along the path of the UE is selected with a margin of 100 m.
2) The thin mesh is solidified by 50 cm.
3) The volume is voxelized with a resolution of 20 cm and adaptivity of 0 cm.
4) The initial texture is rebaked onto the new mesh using Meshlab.

In the second step, the mesh is semantically classified. This entails categorizing each face of the mesh in a number of predefined classes, such as buildings, ground and vegetation. As our method aims to automatically compute the exposure for any location, classification must be performed automatically. With the accelerating capabilities of artificial intelligence, deep-learning semantic classifiers have become sufficiently reliably perform this task for photogrammetry meshes. Both a clean mesh and a texture are essential for the performance of these models. The Semantic Urban Mesh Segmentation (SUMS) deep-learning model features an overall accuracy of 93%. This model is pre-trained on a 4-km^2 area in central Helsinki, Finland. Environments with meshes and textures that do not resemble central Helsinki are expected to yield lower overall accuracies. Therefore, we pick Central Park South Street in New York City, USA, as case-study to examine the extent of overfitting to the training set in the SUMS model. Skyscrapers with a maximal height of 137 m are found south of the street. Central park with a pond is found north of the street.

In the third step, the mesh is planarly decimated with a maximal angle of 5°. This preserves small-scale features such as trees but simplifies large-scale features such as water. Hence, decimation reduces the face count of the considered environment and improves the efficiency of ray-tracing. For each semantic class, a corresponding average material is assigned. The channel and exposure are computed along a path a user takes. For this, a GPX file [8] is created. The input can include two or more addresses, the method of transportation and the velocity of the user. The output is a series of points forming the shortest path between the addresses. A timestamp is assigned to each point such that speed is taken into account. The elevation of the points follows the terrain. We add 1.5 m to this elevation to take the average height of the UE into account.

2) Propagation tool: The path is sampled at a frequency based on the sampling theorem of the Doppler Spectrum. The Rx is modeled as an omnidirectional antenna to provide the input to the hybridization step. Different options are available to place a Tx in the environment. The locations can be assigned randomly as in [10], realistically using open-source data or manually. In the case-study of New York City, a 6G DMaMIMO antenna system operating at 26 GHz is placed on the facade of 50 Central Park South street (see Fig 3). Ray-tracing with shooting and bouncing rays (SBR) was performed with 6 reflections, 0 transmissions and 1 diffraction using Wireless InSite [9]. The collection radius is 85 cm.

3) Hybridizer: The exposure on a virtual phantom is computed using Finite-Difference Time-Domain (FDTD) as in [3]. In previous work, the hybridization procedure between ray-tracing and FDTD is done through a number of saved files for each Angle-of-Arrival (AoA). However, the data required to store the scattered EMFs scales cubically with the frequency. At 26 GHz, the RAM and disk-space requirements are too large to efficiently compute the exposure for a large amount of points along the path. Moreover, spherical wavefronts from nearby sources are not accurately modeled due to the large collection radius in a SBR ray-tracing procedure. We refer to [10] for a comprehensive explanation of the hybridization procedure on a Huygens box. The electric field at the location of the UE is found through the channel of an omnidirectional Rx antenna. This field value normalizes a canonical spherically expanding wave from the Last-Bounce-Scatterer (LBS). The actual LBS is used instead of the quasi-deterministic QuaDRiGa LBS in [10]. The memory requirements now scale quadratically with frequency, making it an ideal method for sub-THz applications. To beamform the signal towards the user, Maximum Ratio Transmission (MRT) precoding is used, assuming no scattering from the UE. Exposure can thus only be accurately assessed when the UE is not near the head of the human phantom.

B. Measurements

The hybridizer from section II-A3 is validated by predicting the EMFs from a measurement in a controlled environment. A DMaMIMO system creates an EMF hotspot in an anechoic room. The NARDA FR2 probe was mounted to a 3D robotic positioner scanning the area around the hotspot. The experiment thus provides the first visual representation and characterization of a 26 GHz hotspot.

1) Transmitting side: The antennas were designed in 2020 for the 5G FR2 band [11]. They are characterized by a small footprint and cost while retaining good performance, as compared to the SOTA. A passive butler matrix system connects to four antenna elements. In 2022, we demonstrated beamforming in 4 distinct directions: -44°, -14°, +14°, +44° [12]. A beam direction is chosen by connecting the correct input to the RF source and matching the other inputs with 50 Ω resistors. Their cost-effective design allows us to build a 16-element DMaMIMO system at 26 GHz for this measurement.

The RF source of 26 GHz enters the room through a sealed cable. The continuous sine signal is split in two with a power-splitter. Both of these signals are then split again with two additional power-splitters. The whole link between RF source and the four outputs is tested with a network analyser. The amplitude of each are the same within 1 to 2 dB. Phase-shifters are added on three of the four inputs. These are passive components that can modulate the phase manually with a mechanical path-length extender. At 11°/GHz, phases can be at most shifted by $3/4\pi$ with a full revolution.

2) Receiving side: NARDA released their FR2 antenna in 2023. The company's product are the SOTA for EMF probes with exposure assessment This measurement constitutes one of the fist experiments with this accurate and easy-to-use equipment. The omnidirectional FR2 probe from NARDA is used as a receiving antenna to measure the EMFs. The probe has an axially symmetric radiation pattern akin to a dipole. The probe measures the electric field component polarized along the length of the probe. Therefore, the probe was oriented orthogonally to the glassfibre pole and parallel to the measuring plane. The electrical signal is processed internally to a field value. This signal is downconverted to a maximum of 6 GHz and connected to NARDA's SRM-3000 with an RF cable. The results are extracted and processed using Python.

3) Configuration: The measurement is performed in an anechoic room covered with RF absorbers. Only the Tx, Rx, 3D positioner and power-splitters are present in the room. The latter is sealed with absorbers and removed as far as possible from the setup. The NARDA FR2 probe is mounted to a 3D scanning system using Velmex positioners [4]. A 2D-scan through the center of the hotspot is performed of size 0.5 m $\times$ 0.5 m, or $44\lambda \times 44\lambda$. The resolution in each direction is 3.33 mm or 0.29λ. Four sets of 4x1 beamforming antenna elements are used. Each is placed on a custom 3D-printed piece that fits the antenna, the cable and the fixture to a glassfibre pole. The pole is placed at a distance of 62 cm parallel to the scanning plane. Its position aligns with the center of the hotspot at $z = 0$ cm. The height of the sets of beamforming antennas are $z =$ -0.52, -0.15, 0.15, 0.52 cm, such that their beamforming angle are 44°, 14°, -14°, -44°, respectively. The directions of the beams converge at the center of the hotspot. However, this setup alone does not guarantee all wavefronts aligning at that location, because the sets have different relative phases. The phase-shifters were manually rotated such that the interference pattern between any two pairs of sets had a maximum at the location of the hotspot. By superposition, the measured electric field component constructively interfered between all sets at the location of the hotspot. This procedure replicates active reciprocity-based beamforming.

4) Validation simulation: The Tx's and Rx's orientation and position are modeled in a free-space environment. Lasers are used to align and position the measurement setup as intended in the simulation to millimeter precision. A full-wave simulation is performed in CST Microwave Studio for the 4x1 beamforming sets, including the attached butler matrix. The far-field patterns for each beam direction are exported to the validation simulation. The Fraunhofer distance of a 4x1 antenna array set is 14.2 cm. Including the butler matrix, it is 95.2 cm. We assume no inter-element correlation between the beamforming sets. Therefore, the total field is simply the sum of each far-field propagated onto the scanning grid using spherically expanding plane waves. The same procedure is applied to the hybridizer.

The absolute value of the orthogonal electric field component is evaluated on the same 2D scanning grid as the measurement. The simulation's resolution is 10 times greater than the measurement's resolution.

III. Results

A. Measurements

The maximal range of $3/4\pi$ for each phase-shifter was found to be sufficient for manual active beamforming. Interference patterns are observed between any two pairs of antenna sets. After tuning the phases, the signal is always

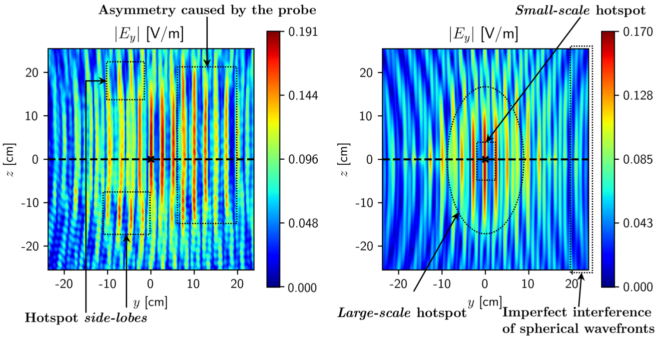

(a) Measurement (b) Simulation

Fig. 2. Comparison of measurement and simulation of a hotspot from a DMaMIMO antenna system in an anechoic room.

maximized at the intended location. The output power of each different beamforming set is different because of the powersplitting. These different amplitudes are measured as 0.022, 0.070, 0.042, 0.035 V/m, starting from the lowest set. A Signal-To-Noise Ratio (SNR) of 12 to 28 dB is observed in the 2D sweep. Measuring at a certain point and moving to the next point takes on average 8 sec. The total measuring time is 50 hours.

A hybridization simulation of this controlled environment was performed. As in real reciprocity-based beamforming, the different amplitudes are taken into account. The channel is renormalized by the measured amplitudes. Thereafter, the channel is precoded using MRT such that the phases align constructively at the hotspot center.

Fig. 2a and 2b shows a 2D slice of the EMFs of the created hotspot by the DMaMIMO system. The absolute value of the electric field component is shown. The hotspot consists of five distinct characteristics. These are highlighted in both figures.

1) A *large-scale* ellipsoidal region of increased EMF compared with the background. This is caused by the alignment of the directions of maximal gain onto the same region. Its size is several wavelengths.
2) Adjacent to this region, small-scale 'side-lobe' of the hotspot are observed of increased EMF compared to their surroundings. These are caused by the constructive interference of a subset of beams. They are wavelength-sized.
3) A *small-scale* constructive interference pattern at the epicenter of the hotspot. The central EMF peak has the highest amplitude and prominence. This is caused by the constructive interference of the wavefronts from each antenna element. It is wavelength-sized.
4) Outside of the hotspot, vertical lines of constructive interference can be seen of increased EMF. The lines are shaped more spherically as their distance from the hotspot center increases. By nature of the geometry, the phases will also align less perfectly as this distance

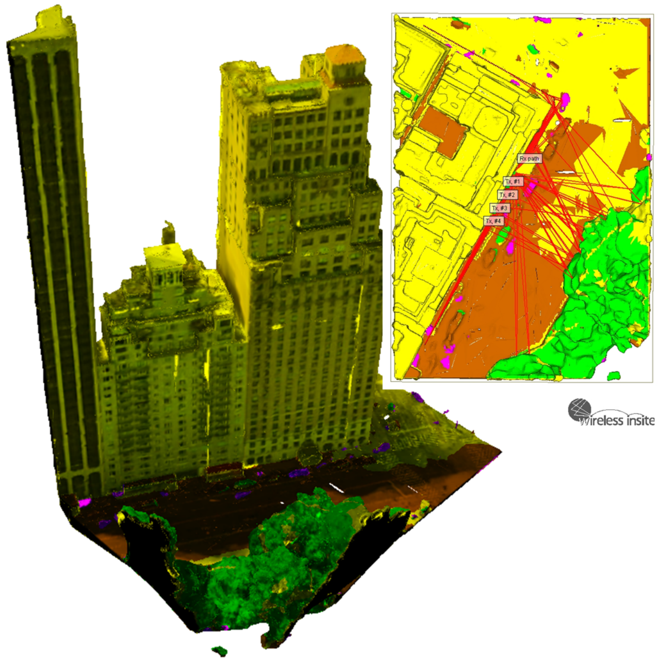

Fig. 3. The processed mesh of Central Park South street in New York City, USA, acquired from from Google Earth. The inset in the top-right corner depicts a ray-tracing simulation.

increases.

5) The hotspot is asymmetrical despit a symmetrical configuration. Field amplitudes are higher to the right of the hotspot. This is attributed by the presence of the measuring probe located at the left of the hotspot. The 48.5 cm FR2 NARDA probe scatters electromagnetic energy to the right of the hotspot. As UE-coupling is neglected in the hybridization component of the pipeline, this asymmetry can not be captured in the simulation.

The one-dimensional slice through the y-axis at $z = 0$ cm is considered. This slice is shown with a dashed black line. The Normalized Mean Absolute Error (NMAE) between measurement and simulation across this slice is 17% $\pm$ 10%, or 0.65 dB. For the simulation, the maximum and Full Width at Half Maximum (FWHM) of the central hotspot peak is 0.17 V/m and 0.94 cm, respectively. For the measurement, the maximum and FWHM of the central hotspot peak is 0.19 V/m and 0.93 cm, respectively. Constructive interference peaks are manually matched. The average height difference between the matched peaks is 6.54% ($\pm$ 28% for the full slice, $\pm$ 5% within the hotspot). The average positional difference between the matched peaks is 0.26%, although this is limited by the measurement's scanning grid resolution of 3.33 mm.

B. Simulations

A picture of the processed mesh is shown in Fig. 3. The deep-learning model performs reasonably well in this new environment.

With the method validated, the full simulation pipeline can be applied on a case-study as in New York. Preliminary testing shows ray-tracing simulations take on average 5 minutes per user. The FDTD simulation takes about 2.5 minutes. A number of S_{ab} are computed as a proof-of-concept of the method. These values are within 1% of the ICNIRP basic restrictions. This indicates ray-tracing the environment is feasible. Full results of this case-study are imminent future work, as this requires large computational resources. Our method will make exposure modeling and exposure-aware network planning a reality in the coming year.

IV. Conclusion

A hybrid ray-tracing/FDTD tool is applied to new 3D Photogrammetry meshes provided by the new Google API. A measurement is performed in an anechoic room to validate a subcomponent of the simulation pipeline. The NMAE between measurement and simulation is 17% in a 1D slice. We also observe 5 characteristics of the hotspot. This allows us to examine a case-study in New York city and prove the feasibility of ray-tracing simulations along a path. Future work will start by computing the results for a number of case studies.

V. Acknowledgements

This work was supported by the ERC through "ATTO: A New Concept for Ultrahigh Capacity Wireless Networks" under Grant 695495 and Methusalem through "SHAPE: Next Generation Wireless Networks".

References

[1] S. Shikhantsov et al., *Numerical Assessment of Human EMF Exposure to Collocated and Distributed Massive MIMO Deployments in an Industrial Indoor Environment*, IEEE Trans. on EMC., vol. 65., no. 4, Aug 2023.

[2] ICNIRP, *Guidelines for limiting exposure to electromagnetic fields (100 kHz to 300 GHz)*, Health Phys 118(00):000–000; 2020. DOI: 10.1097/HP.0000000000001210.

[3] R. Wydaeghe et al., *Realistic Human Exposure at 3.5 GHz and 28 GHz for Distributed and Collocated MaMIMO in Indoor Environments Using Hybrid Ray-Tracing and FDTD*, IEEE Access, vol. 10, Dec 2022.

[4] S. Shikhantsov et al., *Calibrated measurements of the EMF enhancement in the downlink of a 6G distributed antenna array testbed*, URSI GASS 2023.

[5] M. Kleijer et al., *Impact of Facade Details on Radio Propagation at 28 GHz*, European Conference on Ant. and Prop. 2023, Mar. 2023.

[6] R. Heijs et al., *On the Importance of Scattering From Poles in Ray Tracing Simulations*, CA20120, Poznan, Poland, Sep 2023.

[7] Google, *Photorealistic 3D Tiles*, url: https://developers.google.com/maps/documentation/tile/3d-tiles, accessed Oct. 2023.

[8] vvoovv, *Blosm for Blender: OpenStreetMap, Google 3D cities, terrain*, Github, https://github.com/vvoovv/blosm, accessed Oct. 2023.

[9] Remcom, *Wireless InSite*, Software.

[10] R. Wydaeghe et al., *New Hybrid QuaDRiGa-FDTD Method for Realistic Human Exposure Assessment at 28 GHz with 6G Cell-Free Massive MIMO in 3D Outdoor Environments*, *unpublished*.

[11] I. L. de Paula, *Cost-Effective High-Performance Air-Filled SIW Antenna Array for the Global 5G 26 GHz and 28 GHz Bands*, IEEE Ant. and Wire. Prop., vol. 20, no.2, Dec 2020.

[12] L. Van Messem, *A 4 × 4 Millimeterwave-Frequency Butler Matrix in Grounded Co-Planar Waveguide Technology for Compact Integration With 5G Antenna Arrays*, IEEE Tran. on Micr. Theory and Tech., vol. 71, no. 1, Jun. 2022.